New interpretation of the chiral phase transition: Violation of the trilemma in QCD

Chuan-Xin Cui,[*] Jin-Yang Li,[†] and Shinya Matsuzaki[‡]
Center for Theoretical Physics and College of Physics, Jilin University, Changchun 130012, China

Mamiya Kawaguchi[§]
School of Nuclear Science and Technology, University of Chinese Academy of Sciences, Beijing 100049, China

Akio Tomiya[‖]
RIKEN BNL Research center, Brookhaven National Laboratory, Upton, New York 11973, USA and Department of Information Technology, International Professional University of Technology in Osaka, 3-3-1 Umeda, Kita-Ku, Osaka 530-0001, Japan

(Received 9 April 2022; accepted 10 June 2022; published 21 June 2022)

We find that the chiral phase transition (chiral crossover) in QCD at a physical point is triggered by a big imbalance among three fundamental quantities essential for the QCD vacuum structure; susceptibility functions for the chiral symmetry, axial symmetry, and the topological charge. The balance, dobbed the QCD trilemma, is unavoidably violated when one of the magnitudes among them is highly dominated, or suppressed. Based on a three-flavor Nambu-Jona-Lasinio model, we explicitly evaluate the amount of violation of the QCD trilemma at a physical point, and show that the violation takes place not only at vacuum, but even in a whole temperature regime including the chiral-crossover epoch. This work confirms and extends the suggestion recently reported from lattice QCD with two flavors on the dominance of the axial and topological susceptibilities left in the chiral susceptibility at high temperatures. It turns out that the imbalance is essentially due to the flavor symmetry violation of the lightest three flavors, and the flavor breaking specifically brings enhancement of the axial anomaly contribution in the chiral-order parameter, while the strength of the axial breaking and the transition rate of the topological charge are fairly insensitive to the flavor symmetry. The violation of the QCD trilemma and its flavor dependence can be tested by lattice simulations with $2+1$ flavors in the future, and would also give a new guiding principle to explore the flavor dependence of the chiral phase transition, such as the Columbia plot, including a possible extension with external fields.

DOI: 10.1103/PhysRevD.105.114031

I. INTRODUCTION

The chiral phase transition is of importance to comprehend the QCD vacuum, and is also essential to figure out the origin of mass in a view of thermal history of the universe. So far, plenty of studies on the chiral phase transition have extensively been worked out through the nonperturbative analysis in lattice simulations, and also chiral effective models of QCD. However, as argued in the literature [1,2], it still, it is not well understood whether the chiral symmetry breaking is the most dominant source of the origin of mass, even in presence of contamination with the $U(1)_A$ anomaly, and by what mechanism it is restored faster than the $U(1)_A$ symmetry at a high temperature.

The order parameter of the chiral symmetry is given by the quark condensate, which can alternatively be signaled by difference of meson correlation functions for the chiral partners; the latter is referred to as an indicator of the chiral-breaking strength. Despite being so simple and well defined, the chiral-order parameter at a physical point is actually involved, due to finite quark masses, which explicitly break the chiral symmetry. Indeed, the chiral symmetry is restored at high temperatures only in part, referred to as the chiral crossover [3,4]. Actually, it gets more intricate because the chiral-order parameter (the

[*]cuicx1618@mails.jlu.edu.cn
[†]lijy1118@mails.jlu.edu.cn
[‡]synya@jlu.edu.cn
[§]mamiya@ucas.ac.cn
[‖]akio@yukawa.kyoto-u.ac.jp

indicator of the chiral breaking strength) couples with the indicator of the axial breaking strength and topological features of the QCD vacuum via finite quark masses. The latter tagging is captured by a robust relation between the indicators for the chiral $SU(2)_L \times SU(2)_R$ symmetry and $U(1)_A$ axial symmetry, which is constructed from a set of generic anomalous Ward identities for the three-flavor chiral $SU(3)_L \times SU(3)_R$ symmetry [5,6] (for more details, see also the next section),

$$\chi_{\eta-\delta} = \chi_{\pi-\delta} + \frac{4}{m_l^2}\chi_{\rm top}, \tag{1}$$

where $m_l = m_u = m_d$ is the isospin-symmetric mass for the lightest up and down quarks; $\chi_{\eta-\delta} \equiv \chi_\eta - \chi_\delta$ and $\chi_{\pi-\delta} \equiv \chi_\pi - \chi_\delta$ are differences of meson susceptibilities related to the partners for the chiral symmetry (χ_η and χ_δ)—an indicator for the strength of the chiral $SU(2)$ symmetry breaking, and axial symmetry (χ_δ and χ_π)—an indicator for the strength of the $U(1)_A$ axial breaking. $\chi_{\rm top}$ is the topological susceptibility related to the transition rate of the topological charge carried by the QCD θ vaccua. By the chiral $SU(2)$ and axial rotations, the meson susceptibilities exchange their partners; $\chi_\eta \leftrightarrow \chi_\delta$ (chiral) and $\chi_\pi \leftrightarrow \chi_\delta$ (axial), hence $\chi_{\eta-\delta} = 0$ and $\chi_{\pi-\delta} = 0$ are signals of restorations of the associated symmetries. ($\chi_{\rm top} < 0$ and other susceptibilities are positive in our sign convention. See also the next section.) Thus Eq. (1) dictates coherence of the chiral $SU(2)$ symmetry breaking and $U(1)_A$ breaking, linked with the transition rate of the topological charge, where all the breaking is controlled by nonzero quark masses. This anomalous Ward identity takes the same form even in the decoupling limit of strange quarks, i.e., in the lightest two-flavor limit.

Equation (1) plays the essential role in comprehending how the effective restoration of the chiral symmetry is correlated with that of the axial symmetry and the temperature dependence of topological susceptibility in real-life QCD. This gives a new guideline in the sense of exploring the chiral phase transition constrained by Eq. (1), and provides crucial clues to answer the questions posed above.

The lattice QCD simulations with $2+1$ flavors at the physical point have revealed a faster drop of $\chi_{\eta-\delta}$, than $\chi_{\pi-\delta}$ around and above the pseudocritical temperature of the chiral crossover [4]. In the case of two flavors at the chiral limit, the effective restoration of the chiral and axial symmetry has also been discussed through the meson susceptibilities [7–9]

However, those are based on independent measurements of two terms, $\chi_{\eta-\delta}$ and $\chi_{\pi-\delta}$, with the constraint of Eq. (1) disregarded.

Measurements of $\chi_{\rm top}$ on lattice QCD with $2+1$ flavors at around physical point and its temperature dependence have been reported [10–12], in light of detecting the effective restoration of the $U(1)_A$ symmetry assuming the much faster restoration of the chiral $SU(2)$ symmetry. However, those are also individual observations, basically separated from measurements of the chiral and axial indicators. Therefore, it is yet uncovered how the temperature dependence of $\chi_{\rm top}$ would correlate with the other two, with reflecting the constraint of Eq. (1).

In a view of the coherence in Eq. (1), a recent lattice study with two lightest flavors has, for the first time, shown significant contributions from the axial and topological susceptibilities ($\chi_{\pi-\delta}$ and $\chi_{\rm top}$) left in the chiral susceptibility ($\chi_{\eta-\delta}$) in the chiral-crossover domain [2]. This would imply that the faster chiral crossover is triggered by a sizable cancellation between axial and topological susceptibilities, the two terms in the right-hand side of Eq. (1).

To quantify the magnitude of such a cancellation, we may define an ideal case with no preference among three susceptibilities in magnitude in Eq. (1), so that the Ward identity acts like a balance equation. We call this ideal situation the "QCD trilemma", and depict a triangle diagram in Fig. 1. The degree of formation of QCD trilemma can be evaluated via the following quantity,

$$R \equiv \frac{\frac{4}{m_l^2}\chi_{\rm top} + \chi_{\pi-\delta}}{\chi_{\eta-\delta} - \frac{4}{m_l^2}\chi_{\rm top}} = 1 + \frac{\frac{4}{m_l^2}\chi_{\rm top}}{\chi_{\pi-\delta}}. \tag{2}$$

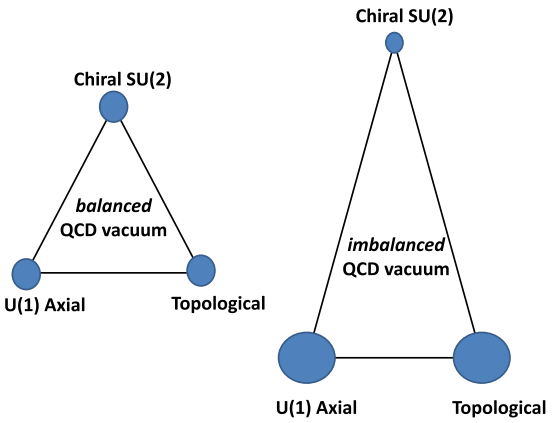

FIG. 1. Illustration of QCD trilemma and its violation. The QCD vacuum structure is built upon the "Chiral SU(2)", "U(1) Axial", and "Topological" features, which are related each other by a balance relation in Eq. (1), where the "Chiral SU(2)", "U(1) Axial", and "Topological" are monitored by $\chi_{\eta-\delta}$, $\chi_{\pi-\delta}$, and $(-4/m_l^2)\cdot\chi_{\rm top}$, respectively. Left panel: the QCD vacuum is "balanced" and holds the trilemma by forming the equilateral triangle with the same order of the weight amplitudes denoted by blobs. Right panel: the trilemma is violated (imbalanced) when a big cancellation between "U(1) Axial", and "Topological" takes place in Eq. (1), which is represented by the isosceles triangle with one blob significantly reduced, keeping Eq. (1) and the corresponding two sides stretched out. As it will be seen in the text, real-life QCD is "imbalanced".

By using this R the Ward identity in Eq. (1) is rewritten as

$$\chi_{\eta-\delta} = R \cdot \chi_{\pi-\delta},$$
$$\text{or} \quad -\frac{4}{m_l^2}\chi_{\text{top}} = (1-R)\cdot\chi_{\pi-\delta}, \tag{3}$$

so that R measures the size of gap in magnitude between the chiral ($\chi_{\eta-\delta}$) and axial ($\chi_{\pi-\delta}$) susceptibilities, or the topological (χ_{top}) and axial ($\chi_{\pi-\delta}$) susceptibilities. Equation (3) tells us that $\frac{\chi_{\eta-\delta}}{\chi_{\pi-\delta}} = R$ and $\frac{(-\frac{4}{m_l^2}\chi_{\text{top}})}{\chi_{\pi-\delta}} = 1-R$, so one may then quantify the amount of balance to keep the QCD trilemma, by saying that the three susceptibilities are balanced when

$$\text{balanced}: \ 0.1 < R < 0.9, \tag{4}$$

otherwise imbalanced along with a big gap of more than one order of magnitude between two of three susceptibilities. An ideal and optimized trilemma is thus realized when $R = 0.5$. We shall dub this R as the trilemma estimator. R becomes $\ll 1$ when axial and topological susceptibilities get close each other with different sign in Eq. (2), which would signal the faster effective restoration of the chiral symmetry than that of the axial one through Eq. (3).

The aforementioned evidence observed by lattice simulations [4] on the faster drop of $\chi_{\eta-\delta}$ than $\chi_{\pi-\delta}$ indicates $R \ll 1$ in a view of Eq. (3). The result from the recent lattice study with the two lightest flavors in [2] can be rephrased as $R \ll 1$ in both Eqs. (2) and (3). Though not explicitly addressed, and restricted only around the crossover regime, this imbalance could also be read off from the existing lattice QCD data with $2+1$ flavors in [4] and also [2] by taking into account possible finite volume effects and statistical errors.

Thus, violation of the QCD trilemma has not been yet explicitly explored at the physical point for $2+1$ flavors on the same lattice setting, and it is still unclear how axial and topological susceptibilities, holding single Eq. (1) with the chiral one, develop in a whole finite-temperature regime and contributes to achieving the chiral crossover. Even in the context of effective chiral models, no such discussion along with Eq. (1) has so far been made together with proper incorporation of the flavor-singlet condition for χ_{top} [6,13,14] (to the latter point, see also the next section). Real-life QCD having $2+1$ flavors at physical point might be imbalanced in realizing the chiral crossover, through undergoing a big cancellation between axial and topological susceptibilities in the whole temperature regime.

In this paper, we discuss the violation of QCD trilemma in real-life QCD based on a Nambu-Jona-Lasinio (NJL) model, and give a qualitative interpretation of the mechanism of the violation, namely the coherence among the chiral, axial, and topological susceptibilities, constrained by Eq. (1). Prior to the lattice simulations, we show that real-life QCD indeed yields $R \ll 1$, i.e., exhibits the violation of QCD trilemma, in the whole temperature regime including the chiral-crossover regime. We find that the violation of the QCD trilemma, and the related dominance of $\chi_{\pi-\delta}$ and χ_{top} in the chiral-order parameter at the crossover regime are due to the three-flavor symmetry violation.

Our findings are testable by lattice simulations, and would help deeper understanding of the flavor dependence of the chiral phase transition, mapped onto the so-called Columbia plot [15]. Exploring the chiral (crossover) phase transition along with the violation of the QCD trilemma would lead to clues toward answering the posed questions; the expected dominance of the chiral symmetry breaking in the origin of mass, and deeper understanding of the observed faster (effective) restoration of the chiral symmetry in the presence of contamination with the $U(1)_A$ anomaly.

This paper is organized as follows. In Sec. II we introduce the preliminaries relevant to the discussion in the later sections, which include definitions and generic formulas for susceptibilities, as well as a concise derivation of the anomalous chiral Ward identity. In Sec. III, the NJL model that we work throughout this paper is introduced, together with showing qualitative consistency of the model predictions with the lattice data, which includes the temperature dependence of the quark condensate, meson susceptibilities, and topological susceptibilities. In Sec. IV we discuss the QCD trilemma estimator R, in a whole temperature region, including the chiral crossover regime, and show the violation of the trilemma, imbalance of the real-life QCD vacuum. We then demonstrate that the violation is due to the three-flavor symmetry. Section V is devoted to our conclusion, where several possible applications of the notion of the QCD trilemma are also briefly addressed.

II. CENTRAL FORMULAS: TOPOLOGICAL SUSCEPTIBILITY AND ANOMALOUS CHIRAL WARD IDENTITIES IN QCD

In this section we begin by reviewing the generic expression for the topological susceptibility χ_{top} [6] with the flavor singlet condition properly reflected [13,14], and introduce the related anomalous chiral Ward identities in QCD involving pseudoscalar susceptibilities χ_π, χ_η and χ_δ.

A. Topological susceptibility: Flavor singlet nature

The topological susceptibility χ_{top} is related to the θ vacuum configuration of QCD. It is defined as the curvature of the θ-dependent vacuum energy $V(\theta)$ in QCD at $\theta = 0$,

$$\chi_{\text{top}} = -\int_T d^4x \left.\frac{\delta^2 V(\theta)}{\delta\theta(x)\delta\theta(0)}\right|_{\theta=0}, \tag{5}$$

where the temperature integral $\int_T d^4x$ is defined as $\int_0^{1/T} d\tau \int d^3x$ with the imaginary time $\tau = ix_0$, and $V(\theta)$

denotes the potential of QCD, which is read off from the generating functional of QCD (in Euclidean space),

$$Z_{\rm QCD} = \int [\Pi_f dq_f d\bar{q}_f][dA] \times \exp\left[-\int_T d^4x \left\{ \sum_{f=u,d,s} (\bar{q}_L^f i\gamma^\mu D_\mu q_L^f + \bar{q}_R^f i\gamma^\mu D_\mu q_R^f + \bar{q}_L^f m_f q_R^f + \bar{q}_R^f m_f q_L^f) + \frac{1}{4g^2}(F_{\mu\nu}^a)^2 + \frac{i\theta}{32\pi^2} F_{\mu\nu}^a \tilde{F}_{\mu\nu}^a \right\}\right]. \quad (6)$$

Here $q_{L(R)}^f$ denote the left-handed and right-handed quark fields; the covariant derivative of the quark field is represented as D_μ involving the gluon fields A, $F_{\mu\nu}^a$ is the field strength of the gluon fields with g being the QCD coupling constant. For simplicity, the quark masses are taken to be real and positive with the electroweak-induced CP violation disregarded.

The form of the θ dependence on the QCD generating functional is ambiguous, because the θ parameter can always be shifted by the $U(1)_A$ rotation through the induced $U(1)_A$ anomaly as well as the phase shift in the quark mass term. Thus the QCD-θ vacuum is shifted by the $U(1)_A$ phase as well. Taking into account this shift, the true QCD vacuum is determined so as to set the net θ to zero, i.e., the CP invariant vacuum, as shown in the context of Vafa-Witten's theorem [16]. The topological susceptibility $\chi_{\rm top}$ should then be evaluated at the true vacuum with the net $\theta = 0$. This is how to properly compute $\chi_{\rm top}$ [14].

Under the $U_A(1)$ rotation with the rotation angle θ_f, the left- and right-handed quark fields are transformed as

$$q_L^f \to \exp(-i\theta_f/2) q_L^f, \quad q_R^f \to \exp(i\theta_f/2) q_R^f. \quad (7)$$

We then find that the extra phase factor shows up in the QCD generating functional written in terms of the transformed chiral quark fields,

$$\int [\Pi_f dq_f d\bar{q}_f][dA] \times \exp\left[-\int_T d^4x \left\{ \sum_{f=u,d,s} (\bar{q}_L^f i\gamma^\mu D_\mu q_L^f + \bar{q}_R^f i\gamma^\mu D_\mu q_R^f + \bar{q}_L^f m_f e^{i\theta_f} q_R^f + \bar{q}_R^f m_f e^{-i\theta_f} q_L^f) + \frac{1}{4g^2}(F_{\mu\nu}^a)^2 + \frac{i(\theta-\bar{\theta})}{32\pi^2} F_{\mu\nu}^a \tilde{F}_{\mu\nu}^a \right\}\right], \quad (8)$$

where $\bar{\theta} = \sum_{f=u,d,s} \theta_f = \theta_u + \theta_d + \theta_s$.

We can take a phase convention in such a way that the θ dependence goes away from the topological gluonic term $(F\tilde{F})$,

$$\theta = \bar{\theta} = \theta_u + \theta_d + \theta_s. \quad (9)$$

Instead, the quark mass term fully carries the θ-dependence, which makes manifest presence of the strong CP violation. Here, the CP-violating phases $\theta_{u,d,s}$ actually involves redundancy, i.e., being not fully independent, because the QCD interaction and the QCD vacuum characterized by the three-flavor symmetric quark condensate are flavor blind (singlet). Therefore, we must recover the flavor independence for those CP-violating phases. Supposing a small enough θ_f (which is to be consistent with the observation on $\theta < 10^{-10}$ from the electric dipole moment of neutron), and expanding the quark mass terms in powers of θ_fs, we find that the CP-violating coupling terms at the nontrivial leading order arise with the factor of $m_f\theta_f$. Thus the desired flavor singlet condition goes like [13],

$$m_u\theta_u = m_d\theta_d = m_s\theta_s \equiv x. \quad (10)$$

By using this flavor singlet condition together with Eq. (9), θ_fs are determined to be proportional to θ as

$$\theta_u = \frac{\bar{m}}{m_u}\theta, \qquad \theta_d = \frac{\bar{m}}{m_d}\theta, \qquad \theta_s = \frac{\bar{m}}{m_s}\theta, \quad (11)$$

where

$$\bar{m} = \left(\frac{1}{m_u} + \frac{1}{m_d} + \frac{1}{m_s}\right)^{-1}. \quad (12)$$

Thus the θ-dependent vacuum energy of QCD with the flavor singlet nature properly reflected is

$$V_{\rm QCD}(\theta) = -\ln\left[\int [\Pi_f dq_f d\bar{q}_f][dA] \exp\left(-\int_T d^4x \mathcal{L}_{\rm QCD}^{(\theta)}\right)\right], \quad (13)$$

where

$$\mathcal{L}_{\rm QCD}^{(\theta)} = \sum_f (\bar{q}_L^f i\gamma^\mu D_\mu q_L^f + \bar{q}_R^f i\gamma^\mu D_\mu q_R^f) + \bar{q}_L \mathcal{M}_\theta q_R + \bar{q}_R \mathcal{M}_\theta^\dagger q_L + \frac{1}{4g^2}(F_{\mu\nu}^a)^2, \quad (14)$$

with $\mathcal{M}_\theta$ being the θ-dependent quark matrix,

$$\mathcal{M}_\theta = \mathrm{diag}\left[m_u \exp\left(i\frac{\bar{m}}{m_u}\theta\right), m_d \exp\left(i\frac{\bar{m}}{m_d}\theta\right), m_s \exp\left(i\frac{\bar{m}}{m_s}\theta\right)\right]. \tag{15}$$

Based on Eq. (13), we evaluate χ_{top} in Eq. (5), and find [6]

$$\begin{aligned}\chi_{\mathrm{top}} &= \bar{m}^2\left[\frac{\langle\bar{u}u\rangle}{m_l} + \frac{\langle\bar{d}d\rangle}{m_l} + \frac{\langle\bar{s}s\rangle}{m_s} + \chi_P^{uu} + \chi_P^{dd} + \chi_P^{ss} + 2\chi_P^{ud} + 2\chi_P^{us} + 2\chi_P^{ds}\right] \\ &= \frac{1}{4}[m_l(\langle\bar{u}u\rangle + \langle\bar{d}d\rangle) + m_l^2(\chi_P^{uu} + \chi_P^{dd} + 2\chi_P^{ud})] \\ &= m_s\langle\bar{s}s\rangle + m_s^2\chi_P^{ss},\end{aligned} \tag{16}$$

where the pseudoscalar susceptibilities $\chi_P^{uu,dd,ud}$, χ_P^{ss}, and $\chi_P^{us,ds}$ are defined as

$$\chi_P^{f_1 f_2} = \int_T d^4x\langle(\bar{q}_{f_1}(0)i\gamma_5 q_{f_1}(0))(\bar{q}_{f_2}(x)i\gamma_5 q_{f_2}(x))\rangle, \quad \text{for } q_{f_{1,2}} = u, d, s. \tag{17}$$

In Eq. (16) we have taken the isospin symmetric limit $m_u = m_d \equiv m_l$. The signs of the quark masses and condensates are chosen to be positive and negative, respectively, such that $\chi_{\mathrm{top}} < 0$. Note that $\chi_{\mathrm{top}} \to 0$, when either of quarks becomes massless (m_l or $m_s \to 0$), reflecting the flavor-singlet nature of the QCD vacuum [13,14].

B. Anomalous chiral Ward identities

The anomalous Ward identities regarding the chiral $SU(3)_L \times SU(3)_R$ symmetry are directly read off from chiral variations of the QCD potential in Eq. (13). The central formula then takes the form

$$\langle\delta_a\mathcal{O}_b(0)\rangle = -\int_T d^4x\langle\mathcal{O}_b(0)\cdot\bar{q}_f(x)i\gamma_5\{T_a, M\}q_f(x)\rangle, \tag{18}$$

where $T_a = \lambda_a/2$ $(a = 1, \ldots, 8)$ are generators of $SU(3)$; δ_a stands for the infinitesimal variation of the chiral $SU(3)$ transformation associated with the generator T_a, under which q_f transforms as $\delta_a q_f = i\gamma_5 T_a q_f$; $\mathcal{O}_b(0)$ $(b = 0, \ldots, 8)$ is an arbitrary operator. In particular, for the pseudoscalar operators $\mathcal{O}_b = \bar{q}_f i\gamma_5 T_b q_f$, choosing $a = 1$, 2, 3, 8 and $b = 0$, 8 with $T_0 = 1/\sqrt{6}\cdot\mathbf{1}_{3\times3}$, we get [5,6]

$$\begin{aligned}\langle\bar{u}u\rangle + \langle\bar{d}d\rangle &= -m_l\chi_\pi, \\ \langle\bar{u}u\rangle + \langle\bar{d}d\rangle + 4\langle\bar{s}s\rangle &= -[m_l(\chi_P^{uu} + \chi_P^{dd} + 2\chi_P^{ud}) - 2(m_s + m_l)(\chi_P^{us} + \chi_P^{ds}) + 4m_s\chi_P^{ss}], \\ \langle\bar{u}u\rangle + \langle\bar{d}d\rangle - 2\langle\bar{s}s\rangle &= -[m_l(\chi_P^{uu} + \chi_P^{dd} + 2\chi_P^{ud}) + (m_l - 2m_s)(\chi_P^{us} + \chi_P^{ds}) - 2m_s\chi_P^{ss}],\end{aligned} \tag{19}$$

where χ_π denotes the pion susceptibility defined as

$$\chi_\pi = \int_T d^4x[\langle(\bar{u}(0)i\gamma_5 u(0))(\bar{u}(x)i\gamma_5 u(x))\rangle_{\mathrm{conn}} + \langle(\bar{d}(0)i\gamma_5 d(0))(\bar{d}(x)i\gamma_5 d(x))\rangle_{\mathrm{conn}}], \tag{20}$$

with $\langle\cdots\rangle_{\mathrm{conn}}$ being the connected part of the correlation function. The form of the anomalous chiral Ward-identities in Eq. (19) will be intact, as long as only the quark masses gives the leading order of explicit chiral-breaking effects, as evident in the chiral variation of Eq. (18).

Combining Ward identities in Eq. (19), we find

$$\chi_{\mathrm{top}} = \frac{1}{2}m_l m_s(\chi_P^{us} + \chi_P^{ds}) = \frac{1}{4}m_l^2(\chi_\eta - \chi_\pi), \tag{21}$$

where χ_η is the eta meson susceptibility, defined as

$$\begin{aligned}\chi_\eta &= \int_T d^4x[\langle(\bar{u}(0)i\gamma_5 u(0))(\bar{u}(x)i\gamma_5 u(x))\rangle + \langle(\bar{d}(0)i\gamma_5 d(0))(\bar{d}(x)i\gamma_5 d(x))\rangle \\ &\quad + 2\langle(\bar{u}(0)i\gamma_5 u(0))(\bar{d}(x)i\gamma_5 d(x))\rangle] \\ &= \chi_P^{uu} + \chi_P^{dd} + 2\chi_P^{ud}.\end{aligned} \tag{22}$$

The last line of Eq. (21) can be written as

$$(\chi_\eta - \chi_\delta) = (\chi_\pi - \chi_\delta) + \frac{4}{m_l^2}\chi_{\mathrm{top}}, \tag{23}$$

where χ_δ is the susceptibility for the delta meson channel (a_0 meson in terms of the Particle Data Group identification), defined in the same way as χ_π in Eq. (17) with the factors of $(i\gamma_5)$ replaced with identity 1. $\chi_{\eta-\delta} \equiv \chi_\eta - \chi_\delta$ and $\chi_{\pi-\delta} \equiv \chi_\pi - \chi_\delta$ play the roles of the indicators to detect the strength of the chiral and axial breaking, which signal the restorations when those (asymptotically) reach zero.

Equation (23) is our central formula, which has been inferred in Eq. (1), and will be explored in details in the later section.

III. A CHIRAL EFFECTIVE MODEL: NJL

In this section we introduce an NJL model that we work on, and give a couple of preliminaries for discussion on the estimate of the QCD trilemma estimator R in Eq. (2), by

showing consistency of the NJL estimates with currently available lattice data on $2+1$ flavors at a physical point. Since the methodology to compute observables and thermodynamic quantities in the model is standard and fully described in a review [17], we will skip all the details, and just present the final formulas directly used to the numerical evaluation of the quark condensates and susceptibilities.

The three-flavor NJL model Lagrangian that we work on is constructed as follows:

$$\begin{aligned}\mathcal{L} &= \bar{q}(i\gamma_\mu\partial^\mu - \mathbf{m})q + \mathcal{L}_{4f} + \mathcal{L}_{\mathrm{KMT}},\\ \mathcal{L}_{4f} &= \frac{g_s}{2}\sum_{a=0}^{8}[(\bar{q}\lambda^a q)^2 + (\bar{q}i\gamma_5\lambda^a q)^2],\\ \mathcal{L}_{\mathrm{KMT}} &= g_D[\det_{i,j}\overline{q_i}(1+\gamma_5)q_j + \mathrm{H.c.}],\end{aligned} \tag{24}$$

where q is the $SU(3)$ triplet-quark field, $q=(u,d,s)^T$. The current quark masses are embedded in the mass matrix $\mathbf{m}$ of the form $\mathbf{m}=\mathrm{diag}(m_u,m_d,m_s)$.

The four-fermion interaction term $\mathcal{L}_{4f}$ is invariant under the chiral $U(3)_L\times U(3)_R$ transformation: $q\to U\cdot q$ with $U=\exp[-i\gamma_5\sum_{a=0}^{8}(\lambda^a/2)\theta^a]$ and the chiral phases θ^a. The mass term in $\mathcal{L}$ explicitly breaks $U(3)_L\times U(3)_R$ symmetry. The determinant term $\mathcal{L}_{\mathrm{KMT}}$, called the Kobayashi-Maskawa-'t Hooft (KMT) [18–21] term, induced from the QCD instanton configuration, preserves $SU(3)_L\times SU(3)_R$ invariance (associated with the chiral phases labeled as $a=1,\ldots,8$) but breaks the $U(1)_A$ (corresponding to $a=0$) symmetry, measured by the effective coupling constant g_D.

The $U(1)_A$ symmetry is anomalous due not only to the quark mass terms, but also the KMT term reflecting the underlying gluonic anomaly. Thus we have the anomalous conservation law,

$$\partial^\mu j_\mu^{a=0} = 2i\overline{q}\mathbf{m}\gamma_5 q - 12g_D\mathrm{Im}[\det\bar{q}_i(1-\gamma_5)q_j]. \tag{25}$$

The matching with the underlying QCD leads to an operator relation; $Q=-4g_D\mathrm{Im}[\det\bar{q}_i(1-\gamma_5)q_j]$, where $Q=g^2/(32\pi^2)F^a_{\mu\nu}\tilde{F}^{a\mu\nu}$ is the topological charge. Using this operator relation together with Eq. (5), one could evaluate χ_{top} as in the literature, e.g., Refs. [22–25] in the framework of the NJL model with the mean-field approximation. However, this procedure makes the flavor-singlet nature of the vacuum nontransparent. The identification of χ_{top} defined within the NJL model with the mean-field approximation with that derived directly in QCD requires a careful separate investigation ensuring the flavor singlet nature of the vacuum in both theories. Instead, in the present paper the NJL model is considered as a reduction of the full QCD allowing the evaluation of the right-hand side of Eq. (16) in which the flavor singlet nature is manifestly built in.

The NJL model itself is a (perturbatively) nonrenormalizable field theory because $\mathcal{L}_{4f}$ and $\mathcal{L}_{\mathrm{KMT}}$ describe the higher-dimensional interactions with mass dimension greater than four. Therefore, a momentum cutoff Λ must be introduced to make the NJL model regularized. We adapt a sharp cutoff regularization for three-dimensional momentum integration, following the literature [17].

A. Gap equations

We employ the mean-field approximation, corresponding to the large N_c limit, and then derive the gap equation and the thermodynamic potential [17]. There the quark condensates (on thermal average) act as the variable of the potential and are T dependent, which we define as

$$\langle\bar{u}u\rangle\equiv\alpha,\qquad \langle\bar{d}d\rangle\equiv\beta,\qquad \langle\bar{s}s\rangle\equiv\gamma. \tag{26}$$

Searching for the minimum point of the thermodynamic potential with respect to α, β, and γ as variational parameters, we find the stationary conditions, corresponding to the gap equations [17,26],

$$\langle\bar{q}_i q_i\rangle = -2N_c\int^{\Lambda}\frac{d^3p}{(2\pi)^3}\frac{M_i}{E_i}[1-2(\exp(E_i/T)+1)^{-1}], \tag{27}$$

where $E_i=\sqrt{M_i^2+p^2}$, N_c denotes the number of colors to be fixed to three, and M_i are full quark masses including the dynamically generated terms,

$$\begin{aligned}M_u &= m_u - 2g_s\alpha - 2g_D\beta\gamma,\\ M_d &= m_d - 2g_s\beta - 2g_D\alpha\gamma,\\ M_s &= m_s - 2g_s\gamma - 2g_D\alpha\beta.\end{aligned} \tag{28}$$

B. Chiral and axial susceptibilities

In this subsection we introduce susceptibilities for pseudoscalar and scalar meson channels and give their explicit formulas in the present NJL model.

1. Pseudoscalar meson channel

In the η–η' coupled channel, the pseudoscalar meson susceptibility is defined on the generator basis as

$$\chi_P^{ij} = \int_T d^4x\langle(i\bar{q}(x)\gamma_5\lambda^i q(x))(i\bar{q}(0)\gamma_5\lambda^j q(0))\rangle, \tag{29}$$

where $i,j=0,8$. This χ_P^{ij} takes a matrix form

$$\chi_P = \frac{-1}{1+G_P\Pi_P(0,0)}\cdot\Pi_P(0,0), \tag{30}$$

where G_P is the coupling strength matrix and Π_P is the polarization-tensor matrix, which are given respectively as

$$G_P = \begin{pmatrix} G_P^{00} & G_P^{08} \\ G_P^{80} & G_P^{88} \end{pmatrix} = \begin{pmatrix} g_s - \frac{2}{3}(\alpha+\beta+\gamma)g_D & -\frac{\sqrt{2}}{6}(2\gamma-\alpha-\beta)g_D \\ -\frac{\sqrt{2}}{6}(2\gamma-\alpha-\beta)g_D & g_s - \frac{1}{3}(\gamma-2\alpha-2\beta)g_D \end{pmatrix}, \quad (31)$$

$$\Pi_P = \begin{pmatrix} \Pi_P^{00} & \Pi_P^{08} \\ \Pi_P^{80} & \Pi_P^{88} \end{pmatrix} = \begin{pmatrix} \frac{2}{3}(2I_P^{uu} + I_P^{ss}) & \frac{2\sqrt{2}}{3}(I_P^{uu} - I_P^{ss}) \\ \frac{2\sqrt{2}}{3}(I_P^{uu} - I_P^{ss}) & \frac{2}{3}(I_P^{uu} + 2I_P^{ss}) \end{pmatrix}, \quad (32)$$

with $I_P^{ii}(\omega, \boldsymbol{p})$ being the pesudoscalar one-loop polarization functions [27],

$$I_P^{ii}(0,0) = -\frac{N_c}{\pi^2}\int_0^\Lambda dp p^2 \frac{1}{E_i}[1 - 2(\exp(E_i/T)+1)^{-1}], \quad \text{for } i = u, d, s. \quad (33)$$

By performing the basis transformation, the pseudoscalar susceptibilities defined in Eq. (17) on the flavor basis are thus obtained as

$$\begin{pmatrix} \frac{1}{2}\chi_P^{uu} + \frac{1}{2}\chi_P^{ud} = \frac{1}{4}\chi_\eta \\ \chi_P^{us} \\ \chi_P^{ss} \end{pmatrix} = \begin{pmatrix} \frac{1}{6} & \frac{\sqrt{2}}{6} & \frac{1}{12} \\ \frac{1}{6} & -\frac{\sqrt{2}}{12} & -\frac{1}{6} \\ \frac{1}{6} & -\frac{\sqrt{2}}{3} & \frac{1}{3} \end{pmatrix} \begin{pmatrix} \chi_P^{00} \\ \chi_P^{08} \\ \chi_P^{88} \end{pmatrix}, \quad (34)$$

where we have taken the isospin symmetric limit into account, i.e., $\chi_P^{uu} = \chi_P^{dd}$ and $\chi_P^{us} = \chi_P^{ds}$.

For χ_π defined in Eq. (17), the explicit formula in the NJL model reads [17]

$$\chi_\pi = \frac{-1}{1 + G_\pi \Pi_\pi(0,0)} \cdot \Pi_\pi(0,0), \quad (35)$$

where $G_\pi = g_s + g_D\gamma$, which is the coupling strength in the pion channel, and Π_π is the quark-loop polarization function for χ_π, which is evaluated by using I_P^{ii} in Eq. (33) as

$$\Pi_\pi = I_P^{uu} + I_P^{dd} = 2I_P^{uu}. \quad (36)$$

2. Scalar meson channel

The definitions of scalar susceptibilities are similar to those for pseudoscalars, which are given just by removing $i\gamma_5$ in the definition of pseudoscalar susceptibilities, and supplying the appropriate one-loop polarization functions and the corresponding coupling constants.

In the 0–8 coupled channel, the scalar susceptibility matrix χ_S is evaluated in the present NJL on the generator basis as

$$\chi_S = \frac{-1}{1 + G_S \Pi_S(0,0)} \cdot \Pi_S(0,0), \quad (37)$$

where G_S is the coupling strength matrix,

$$G_S = \begin{pmatrix} G_S^{00} & G_S^{08} \\ G_S^{80} & G_S^{88} \end{pmatrix} = \begin{pmatrix} g_s + \frac{2}{3}(\alpha+\beta+\gamma)g_D & \frac{\sqrt{2}}{6}(2\gamma-\alpha-\beta)g_D \\ \frac{\sqrt{2}}{6}(2\gamma-\alpha-\beta)g_D & g_s + \frac{1}{3}(\gamma-2\alpha-2\beta)g_D \end{pmatrix}. \quad (38)$$

The scalar polarization tensor matrix Π_S in Eq. (37) is given by

$$\Pi_S = \begin{pmatrix} \Pi_S^{00} & \Pi_S^{08} \\ \Pi_S^{80} & \Pi_S^{88} \end{pmatrix} = \begin{pmatrix} \frac{2}{3}(2I_S^{uu} + I_S^{ss}) & \frac{2\sqrt{2}}{3}(I_S^{uu} - I_S^{ss}) \\ \frac{2\sqrt{2}}{3}(I_S^{uu} - I_S^{ss}) & \frac{2}{3}(I_S^{uu} + 2I_S^{ss}) \end{pmatrix}, \quad (39)$$

with the integral functions,

$$I_S^{ii}(0,0) = -\frac{N_c}{\pi^2}\int_0^\Lambda p^2 dp \frac{E_i^2 - M_i^2}{E_i^3}\{1 - 2[\exp(E_i/T)+1]^{-1}\} \quad i = u, d, s. \quad (40)$$

By moving on to the flavor base via the base transformation, the scalar susceptibilities are cast into the form,

$$\begin{pmatrix} \frac{1}{2}\chi_S^{uu} + \frac{1}{2}\chi_S^{ud} \\ \chi_S^{us} \\ \chi_S^{ss} \end{pmatrix} = \begin{pmatrix} \frac{1}{6} & \frac{\sqrt{2}}{6} & \frac{1}{12} \\ \frac{1}{6} & -\frac{\sqrt{2}}{12} & -\frac{1}{6} \\ \frac{1}{6} & -\frac{\sqrt{2}}{3} & \frac{1}{3} \end{pmatrix} \begin{pmatrix} \chi_S^{00} \\ \chi_S^{08} \\ \chi_S^{88} \end{pmatrix}, \quad (41)$$

in which we have read $\chi_S^{uu} = \chi_S^{dd}$ and $\chi_S^{us} = \chi_S^{ds}$. From this, the σ-meson susceptibility can be also read off as

$$\chi_\sigma = \int_T d^4x [\langle(\bar{u}(0)u(0))(\bar{u}(x)u(x))\rangle + \langle(\bar{d}(0)d(0))(\bar{d}(x)d(x))\rangle + 2\langle(\bar{u}(0)u(0))(\bar{d}(x)d(x))\rangle] = 2\chi_S^{uu} + 2\chi_S^{ud}. \quad (42)$$

We will not directly evaluate this χ_σ in the later section, but it will be inferred when the ambiguity in subtracting the original form of the Ward identity in Eq. (21) by the scalar meson susceptibility, to get the relation between the chiral and axial indicators, and the topological susceptibility (see Sec. IV).

For the δ-meson susceptibility, it is defined as

$$\chi_\delta = \int_T d^4x[\langle(\bar{u}(0)u(0))(\bar{u}(x)u(x))\rangle_{\rm conn} + \langle(\bar{d}(0)d(0))(\bar{d}(x)d(x))\rangle_{\rm conn}]. \quad (43)$$

Similar to χ_π in Eq. (35), the explicit formula for χ_δ reads [17]

$$\chi_\delta = \frac{-\Pi_\delta(0,0)}{1+G_\delta\Pi_\delta(0,0)}, \quad (44)$$

where $G_\delta = g_s - g_D\gamma$, which is the coupling strength in the δ channel, and $\Pi_\delta = I_S^{uu} + I_S^{dd} = 2I_S^{uu}$ is the corresponding quark-loop polarization function.

C. Topological susceptibility in NJL model

Combining Eqs. (21), (30), (31), and (34), we get the formula of $\chi_{\rm top}$ written in terms of the present NJL-model parameters,

$$\begin{aligned}\chi_{\rm top} &= \frac{1}{2}m_l m_s(\chi_p^{us}+\chi_p^{ds}) \\ &= m_l m_s\left(\frac{1}{6}\chi_P^{00} - \frac{\sqrt{2}}{12}\chi_P^{08} - \frac{1}{6}\chi_P^{88}\right) \\ &= \frac{-m_l m_s}{\det(1+G_P\Pi_P)}\left[\frac{1}{6}(\Pi_P^{00}\Pi_P^{88}G_P^{88} - \Pi_P^{082}G_P^{88}) - \frac{\sqrt{2}}{12}(\Pi_P^{082}G_P^{08} - \Pi_P^{00}\Pi_P^{88}G_P^{08}) - \frac{1}{6}(\Pi_P^{88}\Pi_P^{00}G_P^{00} - \Pi_P^{802}G_P^{00})\right] \\ &= \frac{-m_l m_s g_D\alpha}{6\det(1+G_P\Pi_P)}((\Pi_P^{80})^2 - \Pi_P^{88}\Pi_P^{00}). \end{aligned} \quad (45)$$

One can clearly see that $\chi_{\rm top} \propto m_l m_s$, which is reflected by the flavor-singlet nature of the QCD vacuum. Note also that $\chi_{\rm top} \propto g_D$. This should be so because the KMT determinant coupling g_D is directly linked with the gluonic anomaly term in the axial anomaly Eq. (25).

D. NJL estimates

In this subsection we evaluate the temperature dependence of the (subtracted) quark condensate, scalar and pseudoscalar susceptibilities, and the topological susceptibility. We also check the consistency with the recent lattice QCD data on $2+1$ flavors at physical point, and also with other effective models of QCD.

1. Parameter setting

In the present NJL model of Eq. (24), we have five parameters that need to be fixed; the light quark mass m_l, the strange quark mass m_s, the coupling constants g_s and g_D, and the three-momentum cutoff Λ. To fix the parameters, we take the following conservative and empirical input values at $T=0$ in the isospin symmetric limit [17],

$$m_\pi = 136\ \text{MeV}, \quad f_\pi = 93\ \text{MeV}, \quad m_K = 495.7\ \text{MeV}, \quad m_{\eta'} = 957.5\ \text{MeV}. \quad (46)$$

TABLE I. The model parameter setting, followed from [17].

Model parameter description	Input value
Isospin symmetric light quark mass m_l	5.5 MeV
Strange quark mass m_s	138 MeV
Four-fermion coupling constant g_s	0.358 fm^2
Six-fermion coupling constant g_D	−0.0275 fm^5
Cutoff Λ	631.4 MeV

For readers convenience, concise NJL formulas are presented in Appendix. To fix the remaining one degree of freedom, we follow the literature [17,28] to take light quark mass $m_l = 5.5$ MeV (at the renormalization scale of 1 GeV). Thus all the model parameters are fixed, which are presented in Table I.

With the above parameter set,[1] we estimate the topological susceptibility

$$\chi_{\rm top} \simeq 0.025/\text{fm}^4. \quad (47)$$

For this $\chi_{\rm top}$, comparison with the results from the lattice QCD simulations is available, which are $\chi_{\rm top} = 0.019(9)/\text{fm}^4$ [29], and $\chi_{\rm top} = 0.0245(24)_{\rm stat}(03)_{\rm flow}(12)_{\rm cont}/\text{fm}^4$ [12]. Here, for the latter the first error is statistical, the second one comes from the systematic error, and the third one arises due to changing the upper limit of the lattice spacing range in the fit. Although their central values do not agree each other, we may conservatively say that the difference between them is interpreted as a systematic error from the individual lattice QCD calculation.

We will not consider intrinsic-temperature dependent couplings, instead, all the T dependence should be induced only from the thermal quark loop corrections to the

[1]The constituent quark masses are also estimated as $M_u(T=0) = M_d(T=0) \simeq 334.2\,\text{MeV}$, $M_s(T=0) \simeq 530.1\,\text{MeV}$, where use has been made of Eqs. (27)–(28), together with the model parameters listed in Table I.

couplings defined and introduced at vacuum. As it will turn out, the present NJL shows quite good agreement with lattice QCD results on the temperature scaling (normalized to the pseudocritical temperature) for the chiral, axial, and topological susceptibilities. In this sense, we do not need to introduce such an intrinsic T dependence for the model parameters in the regime up to temperatures around the chiral crossover.

2. Subtracted quark condensate

The quark condensate in the NJL model involves a ultraviolet divergence (which is dominated by a quadratic divergence) due to its vacuum part [$\langle -\bar{q}q\rangle \sim N_c m_q \Lambda^2/(4\pi^2)$], and needs to be renormalized when compared with lattice data. Since the quadratic divergences in the quark condensate comes along with current quark masses (as above), we use a subtracted quark condensate as the chiral-order parameter, which has been adopted in the lattice simulations, $\Delta_{l,s}(T) \equiv \langle \bar{l}l\rangle - \frac{m_l}{m_s}\langle \bar{s}s\rangle$, where $\langle \bar{l}l\rangle = \langle \bar{u}u\rangle = \langle \bar{d}d\rangle$.

Figure 2 shows the subtracted quark condensate as a function of temperature predicted from the present NJL model, in comparison with the $2+1$ flavor data from the lattice QCD at the physical point [30]. The pseudocritical temperature $T_{\rm pc}$ is (for the NJL prediction) defined as $d^2\langle \bar{l}l\rangle(T)/dT^2|_{T=T_{\rm pc}} = 0$. We have found $T_{\rm pc}|_{\rm NJL} \simeq 188$ MeV, which is compared with the lattice result $T_{\rm pc}|_{\rm lat} \simeq 155$ MeV [30–34].

In the figure, we have normalized T by their $T_{\rm pc}$. The reason to take the rescaled dimensionless ratios is to make possible systematic errors for the model selection and calculation reduced. For instance, the NJL model predicts somewhat larger T_{pc}, and $\langle \bar{q}q\rangle$ at any T, and basically all dimensionful quantities tend to be overestimated by about 30%; that is thought of as a systematic trend which could be associated with the validity of the large N_c approximation. Then, the dimensionless quantities like T/T_{pc} and $\langle \bar{q}q\rangle_T/\langle \bar{q}q\rangle_{T=0}$ can have reduced systematic errors. So, it would be better to take the rescaled ratios, in order to comprehend how the current effective model can be compatible with the lattice result.

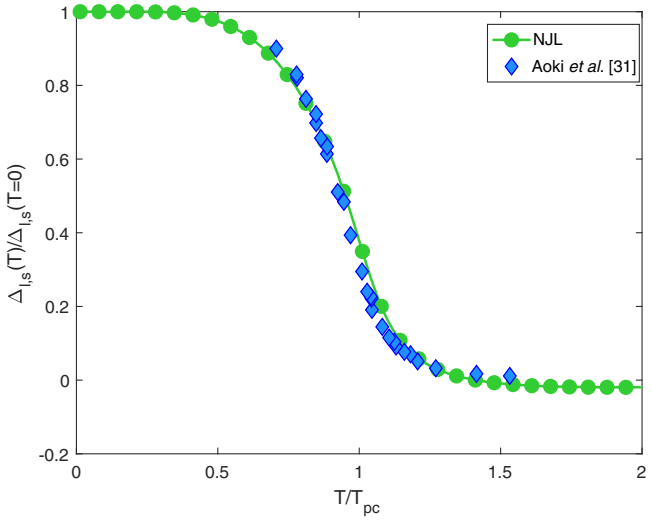

FIG. 2. $T/T_{\rm pc}$ dependence of the subtracted quark condensate, in comparison with data from the lattice QCD with $2+1$ flavors [30]. The normalization factor, the pseudocritical temperature for the chiral crossover ($T_{\rm pc}$) has been set to individual values estimated from the present NJL model ($T_{\rm pc}|_{\rm NJL} \simeq 188$ MeV) and the lattice simulation ($T_{\rm pc}|_{\rm lat} \simeq 155$ MeV).

From Fig. 2, we see that the present NJL prediction is consistent with the lattice data, confirming that the present model describes the chiral-crossover phenomenon quite well.

3. Chiral and axial susceptibility partners

The scalar and pseudoscalar susceptibilities (χ_η, χ_π, χ_σ, χ_δ) presented in Eqs. (34), (35), (42), and (44) are correlated with each other by the chiral $SU(2)_L \times SU(2)_R$ and $U(1)_A$ transformations [35], which can be summarized in the following diagram,

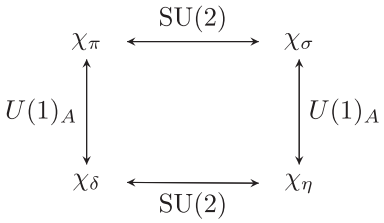

The chiral and axial partners will be degenerate each other in the symmetric limits,

$$\chi_\pi = \chi_\sigma, \quad \chi_\delta = \chi_\eta \quad (\text{chiral } SU(2) \text{ symmetric limit}),$$
$$\chi_\pi = \chi_\delta, \quad \chi_\sigma = \chi_\eta \quad (U(1)_A \text{ axial symmetric limit}). \quad (48)$$

Then, observation of null difference between the above partners can effectively monitor the restoration of the related symmetry. Figure 3 shows the plots of $\chi_{\pi-\delta}/T^2$ (left panel) and $\chi_{\eta-\delta}/T^2$ (right panel) normalized their values measured at $T = T_{\rm pc}$, in comparison to the lattice QCD result [4]. Both of the $T/T_{\rm pc}$ dependence on the normalized susceptibilities show qualitative agreement of the present NJL estimates with the current lattice data.

4. Topological susceptibility

We numerically evaluate $\chi_{\rm top}$ in Eq. (16), with the present NJL estimates on the quark condensates and pseudoscalar susceptibilities, as a function of temperature. In Fig. 4, we plot the temperature dependence of the unnormalized topological susceptibility $\chi_{\rm top}^{1/4}$, where we have taken the absolute value of $\chi_{\rm top}$. Comparison with the dilute instanton gas approximation (DIGA) [36,37], the linear sigma model

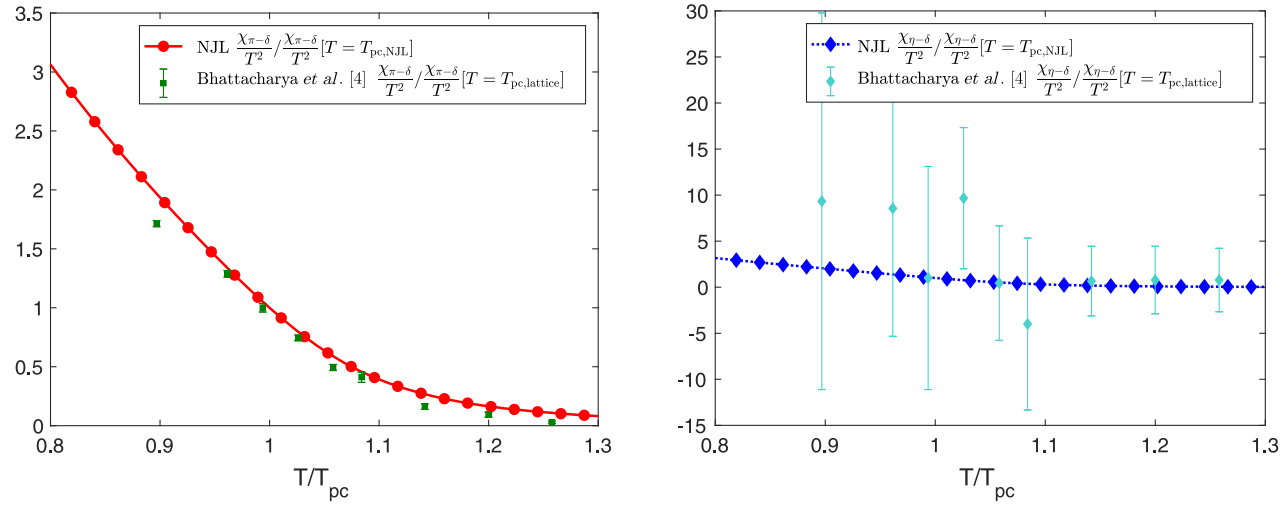

FIG. 3. The normalized susceptibility differences versus temperature normalized by the pseudocritical temperature $T_{\rm pc}$ for the chiral crossover, in comparison with lattice QCD data for $2+1$ flavors [4]. The left panel corresponds to $\chi_{\pi-\delta}/T^2$ divided by its value evaluated at $T=T_{\rm pc}$, and the right panel is the same plots for $\chi_{\eta-\delta}/T^2$. The present NJL yields $T_{\rm pc}|_{\rm NJL}=188$ MeV, and the quoted lattice result predicts $T_{\rm pc}|_{\rm lat}=155$ MeV (at the central value).

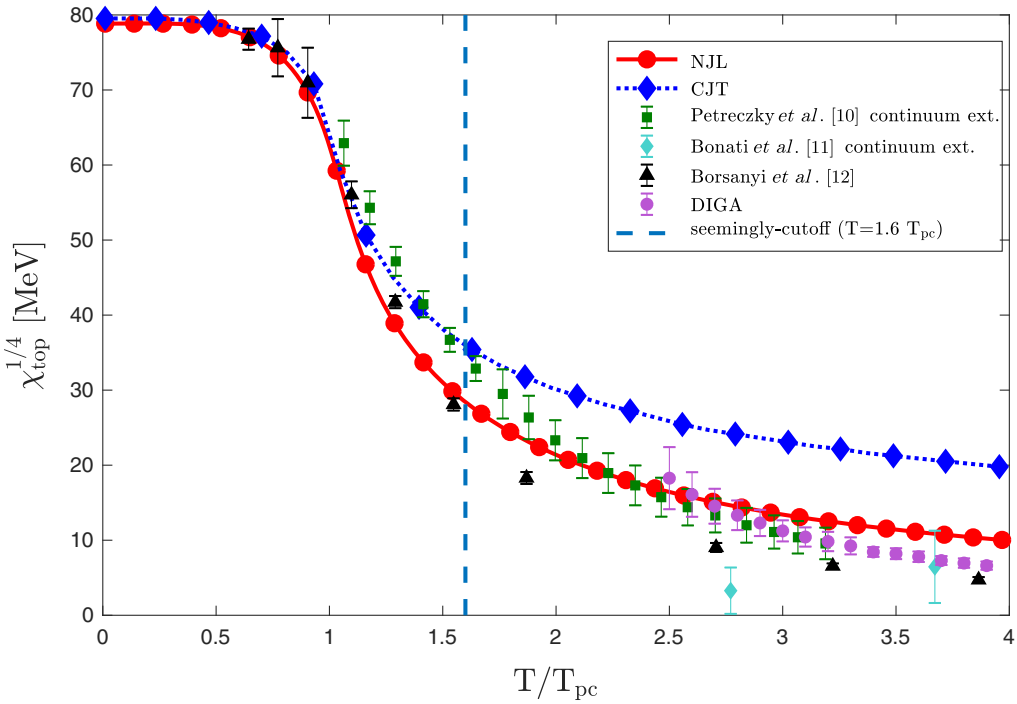

FIG. 4. $T/T_{\rm pc}$ dependence of topological susceptibilities, compared with lattice data [10–12] and other models as described in the text. The vertical line at $T/T_{\rm pc}=1.6$ indicates the theoretical validity of the present NJL model (denoted as the seemingly-cutoff), above which regime the present model description may not be reliable because of lack of the gluonic degrees of freedom (see also footnote 2). This limit needs to be taken into account in referring to the range of $T/T_{\rm pc}$, when compared to the lattice data displayed in the figure.

result (denoted as CJT in the figure) [6] and the result from lattice simulation in the continuum limit [10–12] have also been displayed. The DIGA prediction has been quoted from the literature [10]. For the way of error bars associated with the DIGA, see the cited reference. The temperature is normalized by the pseudo-critical temperature in the figure, where we have taken $T_{\rm pc}|_{\rm NJL}=188$ MeV for the NJL case, $T_{\rm pc}|_{\rm CJT}=215$ MeV for the linear sigma model case, and $T_{\rm pc}|_{\rm lat}=155$ MeV for the lattice.

Figure 4 shows good qualitative agreement between the NJL analysis and lattice result. We see that even though the NJL description without gluonic contribution may not be

reliable for $T/T_{\rm pc} > 1.6$, the good agreement keeps in the whole range of the available lattice data, $T/T_{\rm pc} \sim 0$–4.

At $T < T_{\rm pc}$, all the results fit perfectly with each other, including the linear sigma model estimate. In contrast, when $T > T_{\rm pc}$, we see substantial deviation for the linear sigma model prediction from the NJL's and lattice results.[2] In the literature [6], the pseudoscalar susceptibility terms were not able to evaluate, because the authors did not include the higher-order terms in the current quark masses, and therefore, performing the second-order derivative on the mass parameter to obtain pseudoscalar susceptibility would not be worked out. Thus, their $\chi_{\rm top}$ only includes the quark condensate terms. The present NJL model is able to give the pseudoscalar susceptibility contribution to $\chi_{\rm top}$, to achieve an improved estimate on the quark condensate. The better qualitative agreement of the NJL with the lattice result may thus imply the importance of contributions from the pseudoscalar susceptibilities at higher temperatures, though the model estimate may not rigorously be valid beyond the seemingly cutoff temperature ($T > 1.6T_{\rm pc}$) as noted above.

The topological susceptibility $\chi_{\rm top}$ has been discussed based on the NJL model descriptions similar to ours [22–25]. However, the anomalous Ward identity in Eq. (1) and the flavor-singlet condition necessary in deriving the proper $\chi_{\rm top}$ in Eq. (16) have been ignored there. Absence of the former led to misidentification of the restoration of the axial symmetry, which was played by $\chi_{\rm top}$ in the literature, while the latter missing factor made improper temperature dependence of $\chi_{\rm top}$.

IV. EVALUATION OF QCD TRILEMMA ESTIMATOR

A. Violation of QCD trilemma at physical point in a whole temperature regime

Figure 5 shows values of the trilemma estimator R evolved with T, allowing m_s off the physical point with m_l kept physical. See the middle-solid curve with $m_s = 138$ MeV, which corresponds to real-life QCD. Comparison with the available $2+1$ flavor-lattice QCD data (with $m_\pi = 135$ MeV) on R [4]—reconstructed from the data on $\chi_{\pi-\delta}$ and $\chi_{\eta-\delta}$ through the relation Eq. (3)—has also been displayed (in the zoomed-in window), which shows good agreement including the error bars, for 140 MeV $\lesssim T \lesssim$ 200 MeV. The reconstructed data of R include large errors, which is mainly due to the large uncertainty of the lattice measurement on $\chi_{\eta-\delta}$ (See Fig. 3).

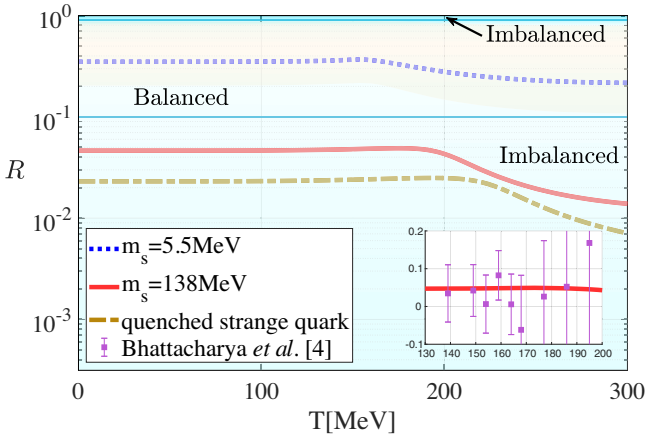

FIG. 5. Plots showing that real-life QCD is imbalanced, which is monitored by the trilemma estimator R defined in Eq. (2). Estimates have been done based on the NJL model described as in the text. Comparison with the $2+1$ flavor-lattice QCD data (with $m_\pi = 135$ MeV) in the available T range has also been displayed with the error bars [4] (in the zoomed-in window). The curve with $m_s = 138$ MeV points to real-life QCD with three flavors, while the quenched-strange quark limit has been achieved by taking $m_s = 50$ GeV, corresponding to the two-flavor limit. Another curve with $m_s = 5.5$ MeV denotes a conjectured prediction in the three-flavor symmetric limit. The "balanced" and "imbalanced" regimes are defined in Eq. (4).

Remarkably, in a whole temperature regime including the chiral crossover regime, real-life QCD stays outside the "balanced" region defined as in Eq. (4). We have observed $R \simeq 0.05$ at around T covering the crossover point ($T_{\rm pc}|_{\rm NJL} \simeq 188$ MeV: 140 MeV $\lesssim T \lesssim$ 200 MeV), consistently with the lattice data, and $R \lesssim 0.01$ at $T \gtrsim 300$ MeV. Namely, the amount of imbalance is slightly amplified by thermal loop effects as T develops from zero.[3]

One might note that subtraction by χ_δ in Eq. (1) is ambiguous, and can be replaced by another chiral susceptibility in the sigma meson channel (χ_σ). We have checked that this replacement does not alter our main conclusion that real-life QCD involves big imbalance. We have also found that $\chi_{\pi-\sigma} \gg \chi_{\eta-\sigma}$ at $T = 0$, $\chi_{\pi-\sigma} \ll \chi_{\eta-\sigma}$ at around the chiral crossover, then $\chi_{\pi-\sigma}$ will get close to $\chi_{\pi-\delta}$, and finally go to zero. The latter trend is consistent with the currently available lattice data [4].

Although the present model parameters are fixed at the physical point, we may deduce some conjectures on the violation of QCD trilemma in a view of the quark mass difference. Extrapolating off real-life QCD, one can then observe that the "imbalanced" domain still covers the two-flavor limit case with $m_s = 50$ GeV (bottom-dot-dashed

[2]Even within the linear sigma model description, it has been also shown that improved treatment of the thermal characteristics of the linear sigma model based on the application of the functional renormalization group technique to the effective potential reproduces quantitatively correctly lattice results for the pseudocritical temperature [38].

[3]Above $T \sim 300$ MeV corresponding to the typical scale of the constituent quark mass, the NJL description as the effective theory of QCD may be somewhat unreliable because the deconfining color degrees of freedom and thermal gluonic contributions would be significant.

curve), where strange quark is decoupled, and the amount of imbalance is greater than that in the real-life QCD case. Taking the three-flavor symmetric limit $m_s = m_l$ with m_l fixed to the physical value, we find "balanced" QCD (top-dashed curve), which keeps almost constant R at any finite T within the "balanced" interval in Eq. (4). This implies that the three-flavor symmetry would be related to the relaxation of the QCD trilemma.

B. QCD trilemma and flavor symmetry

Since the order of magnitude for R tends to be almost fixed at $T = 0$, we may focus only on R at $T = 0$, and look into the flavor-symmetry dependence on R, by varying m_s in a wide range, with fixed m_l to the physical value. Figure 6 shows plots on R as a function of m_s/m_l, together with the "balanced" interval in Eq. (4). As m_s goes off the flavor symmetric limit in the "balanced" domain to be smaller, R tends to get larger, to flow into the "imbalanced" domain with gigantically suppressed $\chi_{\rm top}$. The figure clearly shows that "balanced" QCD should have had some approximate three-flavor symmetry for up, down and strange quarks with $0.06 \lesssim m_s/m_l \lesssim 6$.

We shall investigate the dependence of the flavor-symmetry violation on the imbalanced QCD trilemma in more details. First of all, we may simply suppose that the scalar and pseudoscalar susceptibilities are scaled with the associated meson masses,[4] like $\chi_\delta \propto 1/m_\delta^2$, $\chi_\eta \propto 1/m_\eta^2$ and $\chi_\pi \propto 1/m_\pi^2$, and consider the light quark mass m_l to generically differ from the strange quark mass m_s, including the real-life QCD case with the three-flavor symmetry broken. Among the susceptibilities, χ_π is most sensitive to the current mass of the light quarks (m_l), because the pion is the pseudo-Nambu-Goldstone boson of spontaneous breaking of $SU(2)_L \times SU(2)_R$ symmetry carried by the light quarks. The χ_π thus monotonically gets smaller (larger), as m_l gets larger (smaller), by following $\chi_\pi \propto 1/m_\pi^2 \sim 1/m_l$. On the other hand, the other pseudoscalar susceptibility χ_η significantly involves the U(1)-axial anomaly contribution in m_η, so it almost keeps constant in m_l. The scalar susceptibility χ_δ, free from the Nambu-Goldstone boson nature, also keeps constant with the change of m_l. Besides, the topological susceptibility $\chi_{\rm top}$ also simply scales with m_l, respecting the flavor-singlet condition, $\chi_{\rm top} \to 0$ as $m_l \to 0$, and will be completely constant in m_l for $m_l > m_s$ due to decoupling of the "light" quarks. Thus the difference in magnitude of susceptibilities are simply originated from the scaling properties with respect to the current mass of the light quarks. We plot those m_l scaling behaviors (at $T = 0$) in Fig. 7. The light quark mass is allowed to vary from 10^{-2} eV to the cutoff scale of the presently employed NJL model (631.4 MeV), since the result from m_l above the cutoff scale would be of poor reliability. From the figure, the m_l dependence is read off and the susceptibilities are found to take simple power laws when $m_l \lesssim m_s$,

$$\begin{aligned} &\chi_\pi \sim m_l^{-1}, \\ &\chi_\eta \sim \text{constant}, \quad \text{for } m_l < m_s, \\ &\chi_\delta \sim \text{constant}, \quad \text{for } m_l < m_s, \\ &\chi_{\rm top} \sim m_l, \quad \text{for } m_l < m_s. \end{aligned} \tag{49}$$

Next, consider the three-flavor symmetric limit, where $m_l = m_s$. In this case QCD is balanced as noted above. It also turns out that the scaling law of χ_η in Eq. (49) is broken: the Ward identity Eq. (21) tells us that the difference between χ_π and χ_η is controlled by the $4\frac{m_s}{m_l}\chi_P^{ls}$ term (where $\chi_P^{ls} = \chi_P^{us} = \chi_P^{ds}$). Since no preference among quark flavors is present in the flavor symmetric case, χ_P^{ls} should be on the same order of magnitude as that of χ_π, which we

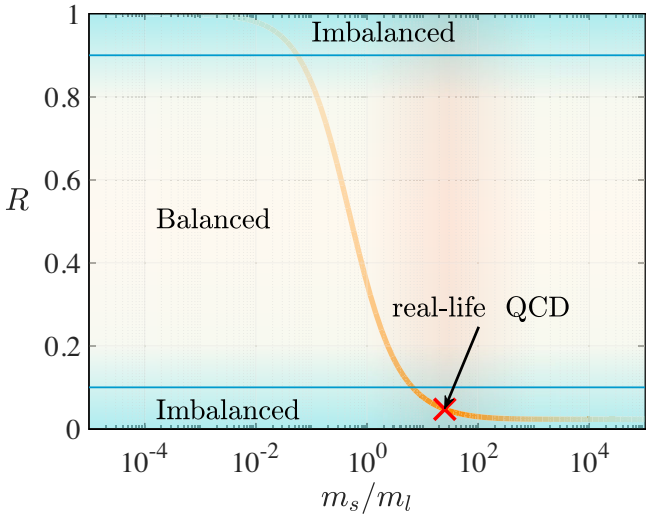

FIG. 6. Plots on the QCD trilemma estimator R at $T = 0$ as a function of m_s/m_l, along with the "balanced" interval defined in Eq. (4). The shaded domain surrounded by the real-life QCD point implies confidence level intervals for the model prediction, where the model parameters, except for m_s, have been fixed at the physical point, as noted in the text. The thinner-shaded regions should be understood as indefinitely extrapolated results with somewhat poor reliability.

[4]The susceptibilities correspond to meson-correlation functions at zero momentum transfer. This is in contrast to the conventional meson correlators depending on the transfer momentum, from which meson masses are read off. Furthermore, the susceptibilities involve contact term contributions independent of momenta, which could be sensitive to a high-energy scale physics, while the conventional meson correlators are dominated by the low-lying meson mass scale. Nevertheless, the degeneracy of the chiral or axial partners at high temperatures, similar to those detected in the susceptibility, can also be seen in the mass difference or equivalently the degeneracy of the conventional meson correlators for the partners, which is simply because the mass difference plays an alternative indicator of the chiral or axial breaking as observed in the lattice simulations [39,40].

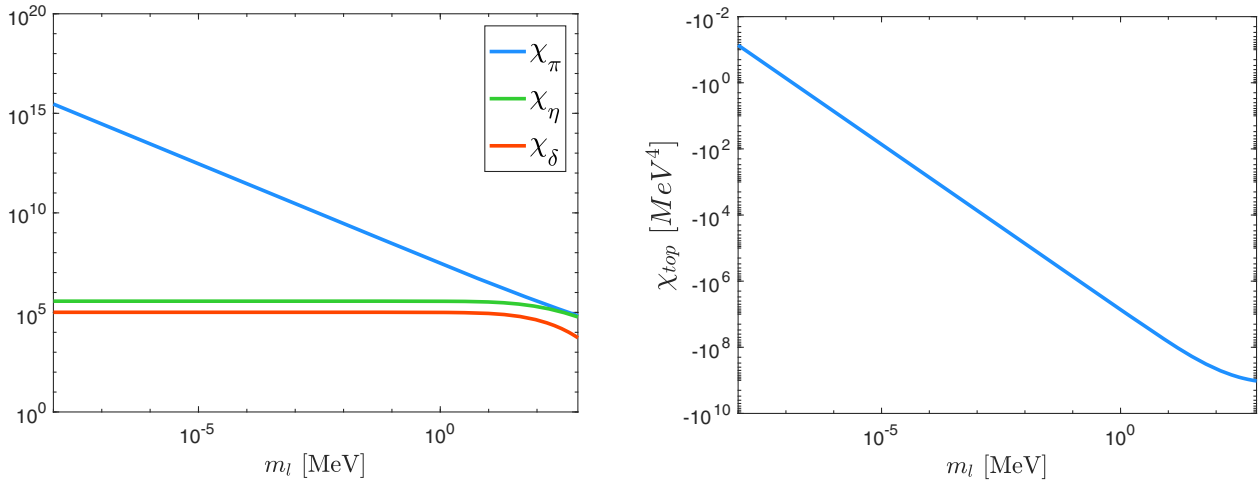

FIG. 7. (Without the three-flavor symmetry): the m_l dependence on χ_π, χ_η, χ_δ [MeV^2] (left panel), and $\chi_{\rm top}$ [MeV^4] (right panel) at $T = 0$. The value of strange quark mass m_s is fixed to be equal to m_l in the plots.

have indeed numerically confirmed. See Fig. 8. Since $m_l = m_s$, there is no extra power scaling of $1/m_l$ which is present in the flavor asymmetric case and leads to a big enhancement of the $(4\frac{m_s}{m_l}\chi_P^{ls})$ part to destructively interfere with χ_π, yielding a much suppressed χ_η compared to χ_π (see Fig. 7). Thus the scaling law of χ_η is the same as that of χ_π, i.e., $\chi_\eta \sim m_l^{-1}$, while others take the same scaling laws as in Eq. (49), namely,

$$\begin{aligned} \chi_\pi \sim \chi_\eta \sim m_l^{-1} \quad & \text{for } m_l = m_s, \\ \chi_\delta \sim \text{constant} \quad & \text{for } m_l = m_s, \\ \chi_{\rm top} \sim m_l \quad & \text{for } m_l = m_s, \end{aligned} \tag{50}$$

as depicted in Fig. 8.

This scaling violation in the flavor symmetric case can also be understood as a big suppression of the $U(1)_A$ anomaly contribution, coupled to the flavor violation, to m_η^2, which dominates in χ_η in the flavor asymmetric case: in the flavor symmetric case we have $\chi_\pi = \chi_P^{88}$, and $\chi_\eta = \chi_\pi + 4\chi_P^{ls}$ with $\chi_P^{ls} = 1/6(\chi_P^{00} - \chi_P^{88})$. Straightforward numerical evaluation reveals that $\chi_P^{88} \gg \chi_P^{00}$ for small m_l. Then, we find $\chi_\eta \approx \chi_\pi/3 \sim 1/m_l$ for small m_l. In particular, note that $\chi_P^{88} = \chi_\pi$ does not include the $U(1)_A$ anomaly effect, and is now much larger than the $U(1)_A$-anomaly affected χ_P^{00} part, which implies the $U(1)_A$ anomaly contribution is much suppressed in χ_η, hence in m_η as well.

Thus the three-flavor symmetry brings the m_l scaling universal among susceptibilities for the pion and eta meson, by suppressing the $U(1)_A$ anomaly contribution only in the eta meson channel. This, on the other side of the same coin,

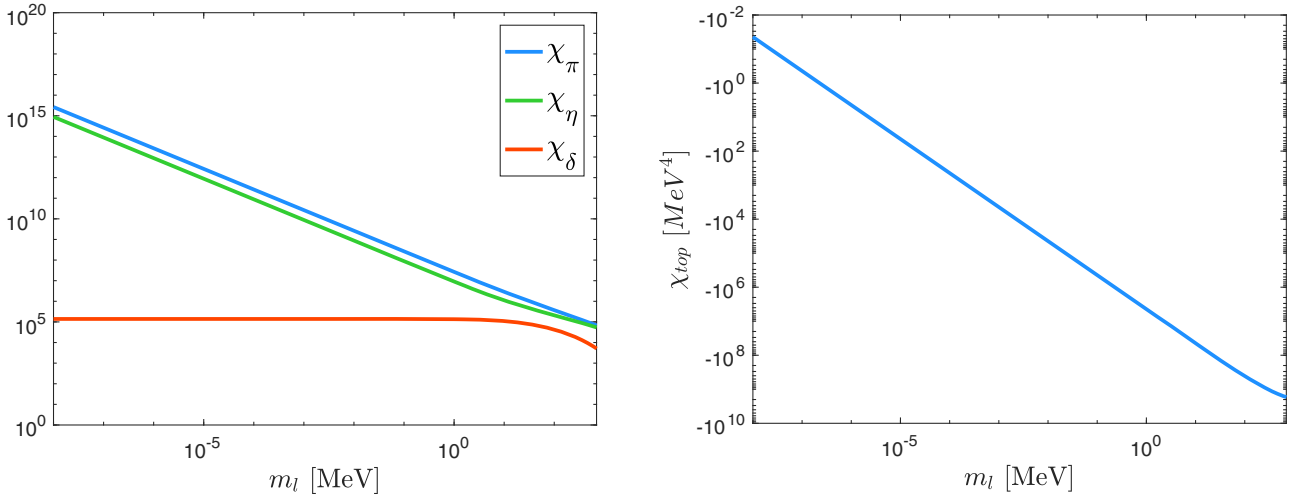

FIG. 8. (With the three-flavor symmetry): The same plots as those in Fig. 7, but with the three-flavor symmetry, where $m_s = m_l$.

indicates that the amplification of the $U(1)_A$ anomaly effect in $\chi_{\eta-\delta}$ so that the chiral symmetry is more quickly restored than the axial symmetry with holding the anomalous chiral Ward identity Eq. (1).

V. CONCLUSION

In conclusion, real-life QCD is required to relax the trilemma ($R \ll 1$), meaning that the much smaller strength of the chiral breaking is given by a big cancellation between the strength of the axial breaking and the transition rate of the topological charge. This is schematically depicted in Fig. 1. This is "imbalance" of the QCD vacuum, present in a whole temperature regime of thermal QCD including the vacuum at $T = 0$. This imbalance or violation of QCD trilemma is triggered due to the three-flavor symmetry violation for up, down and strange quarks, in particular the lightness of up and down quarks. The violation of the three-flavor symmetry specifically brings enhancement of the $U(1)_A$ anomaly contribution in the chiral $SU(2)$ breaking to be insensitive to the smallness of the light quark mass, while the axial indicator and the transition rate of the topological charge are fairly insensitive to the flavor symmetry—in other words, the flavor symmetry dramatically suppresses the $U(1)_A$ anomaly effect in the chiral $SU(2)$ breaking. This implies that in the QCD vacuum with the trilemma realized, all the three-flavor octet pseudoscalar mesons act like identical pseudo Nambu-Goldstone bosons, so that the chiral and axial breaking together with the topological charge contribute to the QCD vacuum on the same order of magnitude.

The present work confirms and extends the suggestion recently reported from lattice QCD with two flavors on dominance of the axial and topological susceptibilities left in the chiral susceptibility at high temperatures over the chiral crossover [2].

The violation of QCD trilemma would be crucial to deeply pursue the expected dominance of the chiral symmetry breaking in the origin of mass, and provides the understanding of mechanism how the faster (effective) restoration of the chiral symmetry in the presence of contamination with the $U(1)_A$ anomaly is achieved; it is understood as a big cancellation between the axial and topological susceptibilities, due to the three-flavor violation among up, down and strange quarks. Our findings can directly be tested on lattice QCD with $2+1$ flavors at physical point and also off physical point, in the future.

It would be nice if the violation of QCD trilemma could be evaluated directly using lattice QCD, but since the quark masses need to be varied, the lattice calculation is so costly. As the first step, it would be appropriate to perform the calculation using a conventional effective model like the present NJL. In fact, it has been shown that the present NJL model matches the lattice results on a couple of observables relevant to the chiral crossover regime, within a deviation of about 30% (consistent with the expected theoretical uncertainty of the large N_c/mean field approximation on that the present NJL is built). This shows that the present NJL model, though being based on the rough mean field approximation, indeed is even quantitatively valid as an effective model of QCD, as good as the lattice QCD. Thus the present work gives motivation to the research in other QCD-compatible theories, such as lattice and/or functional renormalization group approach.

In closing, we give several comments related to possible applications of concept of QCD trilemma:

(i) The notion of QCD trilemma and its violation would also provide us with a new guiding principle to explore the flavor dependence of the chiral phase transition, such as the Columbia plot [15].

(ii) It would be also intriguing to study the violation of QCD trilemma, by means of the nonperturbative renormalization group.

(iii) Correlations between the violation of QCD trilemma and deconfinement-confinement phase transition can be addressed, when the present NJL model is extended by including the Polyakov loop terms.

(iv) Since the form of the anomalous chiral Ward identity in Eq. (1) will be intact as long as the quark mass terms are only the leading source to explicitly break the three-flavor chiral symmetry, the presently described argument would possibly be applicable also to dense QCD, and thermomagnetic QCD, where in the latter case the electromagnetic interactions contribute as the subleading (loop) order to the chiral breaking, as in Eq. (18).

Those will deserve to another publication.

ACKNOWLEDGMENTS

We thank Tetsuo Hatsuda for giving us a crucial comment on the susceptibilities, and are also grateful to Hidenori Fukaya for a fruitful discussion. This work was supported in part by the National Science Foundation of China (NSFC) under Grants No. 11747308, No. 11975108, and No. 12047569, and the Seeds Funding of Jilin University (S. M.). The work of A. T. was supported by the RIKEN Special Postdoctoral Researcher program and partially by JSPS KAKENHI Grant No. JP20K14479.

APPENDIX: NJL FORMULAS

In this appendix we list the NJL formulas used for the inputs observables in Eq. (46), which can be found in Ref. [17]:

(i) The pion decay constant f_π: it is computed by directly evaluating quark loop contributions to the spontaneously broken $SU(2)$ axial current $J_\mu^{A,a} = \bar{l}\gamma_\mu\gamma_5(\sigma^a/2)l$ $(a = 1, 2, 3)$, through the definition of f_π, $\langle 0|J_\mu^{Aa}(0)|\pi^b(p)\rangle = -ip_\mu f_\pi \delta^{ab}$. In the NJL model with the large N_c limit taken (summing up the ring diagrams), we thus have

$$f_\pi = G_{\pi q}(m_\pi) M_u \frac{2N_c}{\pi^2}\int_0^\Lambda dp \times \frac{p^2}{\sqrt{M_u^2+p^2}[4(M_u^2+p^2)-m_\pi^2]}, \quad \text{(A1)}$$

where $G_{\pi q}(p=m_\pi)$ is the pion wavefunction renormalization amplitude evaluated at the onshell,

$$G_{\pi q}^2(m_\pi) = \left(\frac{N_c}{2\pi^2}\int_0^\Lambda p^2 dp \frac{\sqrt{M_u^2+p^2}}{(p^2+M_u^2-\frac{m_\pi^2}{4})^2}\right)^{-1}. \quad \text{(A2)}$$

(ii) The pion mass m_π is computed by extracting the pole of the pion propagator dynamically generated by the quark loop contribution in the NJL with a resummation technique (random phase approximation) applied [17]. The pole position is thus detected as

$$1 + G_\pi \Pi_\pi(m_\pi^2) = 0. \quad \text{(A3)}$$

This pion mass is actually related to the light quark condensate, via the low energy theorem (the so-called Gell-Mann-Oakes-Renner relation):

$$m_\pi^2 = -2m_l\langle \bar{l}l\rangle / f_\pi^2. \quad \text{(A4)}$$

(iii) The kaon mass m_K is calculable in the same way as in the case of m_π above:

$$1 + G_K \Pi_K(m_K^2) = 0, \quad \text{(A5)}$$

where

$$G_K = g_s + g_D\langle \bar{u}u\rangle, \quad \text{(A6)}$$

$$\Pi_K(w) = 2F(w;u,s) + 2F(-w;s,u), \quad \text{(A7)}$$

$$F(w;i,j) = -\frac{N_c}{4\pi^2}\int_0^\Lambda p^2 dp \left[\frac{1}{E_i} f_{ij}(w) + \frac{1}{E_j} f_{ji}(w)\right], \quad \text{(A8)}$$

$$f_{ij}(w) = 2\frac{M_i(M_j - M_i) - E_i w}{E_j^2 - (E_j + w)^2}. \quad \text{(A9)}$$

(iv) The η' mass $m_{\eta'}$ is identified as the highest mass eigenvalue arising from the mass mixing in the 0–8 channel. Similarly to the pion and kaon cases, $m_{\eta'}$ is then extracted by the highest pole of the mixed propagator in the 0–8 channel, $D(q^2)$, as

$$D_{\eta'}(m_{\eta'}^2) = 0, \quad \text{(A10)}$$

where

$$D(q^2) = -G_P^{-1}\left(\frac{1}{1+G_P\Pi^P(q^2)}\right) \equiv \begin{pmatrix} A(q^2) & B(q^2) \\ B(q^2) & A(q^2)\end{pmatrix}, \quad \text{(A11)}$$

through the diagonalization process like

$$T_\theta D^{-1}(q^2) T_\theta^{-1} = \begin{pmatrix} D_{\eta'}^{-1}(q^2) & 0 \\ 0 & D_\eta^{-1}(q^2)\end{pmatrix}. \quad \text{(A12)}$$

Here $\Pi^P(q^2)$ is a function given as the generalization of Eq. (32) with the replacement of the loop function $I_{ii}^P(w^2)$,

$$I_{ii}^P(w^2) = -\frac{4N_c}{\pi^2}\int_0^\Lambda p^2 dp \frac{E_i}{4E_i^2 - w^2}, \quad \text{(A13)}$$

and T_θ is the diagonalization matrix,

$$T_\theta = \begin{pmatrix} \cos(\theta) & -\sin(\theta) \\ \sin(\theta) & \cos(\theta)\end{pmatrix}, \quad \tan(2\theta) = \frac{2B(q^2)}{C(q^2) - A(q^2)}. \quad \text{(A14)}$$

[1] E. V. Shuryak, Comments Nucl. Part. Phys. **21**, 235 (1994).
[2] S. Aoki, Y. Aoki, H. Fukaya, S. Hashimoto, C. Rohrhofer, and K. Suzuki (JLQCD Collaboratuon), Prog. Theor. Exp. Phys. **2022**, 023B05 (2022).
[3] Y. Aoki, G. Endrodi, Z. Fodor, S. D. Katz, and K. K. Szabo, Nature (London) **443**, 675 (2006).
[4] T. Bhattacharya, M. I. Buchoff, N. H. Christ, H. T. Ding, R. Gupta, C. Jung, F. Karsch, Z. Lin, R. D. Mawhinney, G. McGlynn *et al.*, Phys. Rev. Lett. **113**, 082001 (2014).
[5] A. Gómez Nicola and J. Ruiz de Elvira, J. High Energy Phys. 03 (2016) 186.
[6] M. Kawaguchi, S. Matsuzaki, and A. Tomiya, Phys. Rev. D **103**, 054034 (2021).

[7] T. D. Cohen, Phys. Rev. D **54**, R1867 (1996).
[8] T. D. Cohen, arXiv:nucl-th/9801061.
[9] S. Aoki, H. Fukaya, and Y. Taniguchi, Phys. Rev. D **86**, 114512 (2012).
[10] P. Petreczky, H. P. Schadler, and S. Sharma, Phys. Lett. B **762**, 498 (2016).
[11] C. Bonati, M. D'Elia, G. Martinelli, F. Negro, F. Sanfilippo, and A. Todaro, J. High Energy Phys. 11 (2018) 170.
[12] S. Borsanyi, Z. Fodor, J. Guenther, K. H. Kampert, S. D. Katz, T. Kawanai, T. G. Kovacs, S. W. Mages, A. Pasztor, F. Pittler *et al.*, Nature (London) **539**, 69 (2016).
[13] V. Baluni, Phys. Rev. D **19**, 2227 (1979).
[14] J. E. Kim, Phys. Rep. **150**, 1 (1987).
[15] F. R. Brown, F. P. Butler, H. Chen, N. H. Christ, Z. h. Dong, W. Schaffer, L. I. Unger, and A. Vaccarino, Phys. Rev. Lett. **65**, 2491 (1990).
[16] C. Vafa and E. Witten, Nucl. Phys. **B234**, 173 (1984).
[17] T. Hatsuda and T. Kunihiro, Phys. Rep. **247**, 221 (1994).
[18] M. Kobayashi and T. Maskawa, Prog. Theor. Phys. **44**, 1422 (1970).
[19] M. Kobayashi, H. Kondo, and T. Maskawa, Prog. Theor. Phys. **45**, 1955 (1971).
[20] G. 't Hooft, Phys. Rev. Lett. **37**, 8 (1976).
[21] G. 't Hooft, Phys. Rev. D **14**, 3432 (1976); **18**, 2199(E) (1978).
[22] K. Fukushima, K. Ohnishi, and K. Ohta, Phys. Rev. C **63**, 045203 (2001).
[23] P. Costa, M. C. Ruivo, C. A. de Sousa, H. Hansen, and W. M. Alberico, Phys. Rev. D **79**, 116003 (2009).
[24] Y. Jiang and P. Zhuang, Phys. Rev. D **86**, 105016 (2012).
[25] Y. Jiang, T. Xia, and P. Zhuang, Phys. Rev. D **93**, 074006 (2016).
[26] T. Kunihiro and T. Hatsuda, Prog. Theor. Phys. **71**, 1332 (1984).
[27] T. Kunihiro, Nucl. Phys. **B351**, 593 (1991).
[28] G. A. Miller, B. M. K. Nefkens, and I. Slaus, Phys. Rep. **194**, 1 (1990).
[29] C. Bonati, M. D'Elia, M. Mariti, G. Martinelli, M. Mesiti, F. Negro, F. Sanfilippo, and G. Villadoro, J. High Energy Phys. 03 (2016) 155.
[30] Y. Aoki, S. Borsanyi, S. Durr, Z. Fodor, S. D. Katz, S. Krieg, and K. K. Szabo, J. High Energy Phys. 06 (2009) 088.
[31] S. Borsanyi, G. Endrodi, Z. Fodor, C. Hoelbling, S. Katz, S. Krieg, C. Ratti, and K. Szabo (Wuppertal-Budapest Collaboration), J. Phys. Conf. Ser. **316**, 012020 (2011).
[32] H. T. Ding, F. Karsch, and S. Mukherjee, Int. J. Mod. Phys. E **24**, 1530007 (2015).
[33] A. Bazavov *et al.* (HotQCD Collaboration), Phys. Lett. B **795**, 15 (2019).
[34] H. T. Ding, Nucl. Phys. **A1005**, 121940 (2021).
[35] A. Bazavov *et al.* (HotQCD Collaboration), Phys. Rev. D **86**, 094503 (2012).
[36] R. D. Pisarski and L. G. Yaffe, Phys. Lett. **97B**, 110 (1980).
[37] D. J. Gross, R. D. Pisarski, and L. G. Yaffe, Rev. Mod. Phys. **53**, 43 (1981).
[38] G. Fejös and A. Patkos, Phys. Rev. D **105**, 096007 (2022).
[39] B. B. Brandt, A. Francis, H. B. Meyer, O. Philipsen, D. Robaina, and H. Wittig, J. High Energy Phys. 12 (2016) 158.
[40] B. B. Brandt, O. Philipsen, M. Cè, A. Francis, T. Harris, H. B. Meyer, and H. Wittig, Proc. Sci., CD2018 (**2019**) 055.